Iron–sepiolite magnetorheological fluids with improved performances

Jessica A Marins, Tomáš Plachý, Pavel Kuzhir

Iron - sepiolite magnetorheological fluids with improved performances

Jessica A. Marins[1], Tomáš Plachý[1,2], and Pavel Kuzhir[1*]

[1] University Côte d'Azur, CNRS UMR 7010 Institute of Physics of Nice, Parc Valrose 06108 Nice, France

[2] Centre of Polymer Systems, Tomas Bata University in Zlin, trida Tomase Bati 5678, 760 01 Zlin, Czech Republic

***** Corresponding author: kuzhir@unice.fr

Abstract

This work is focused on the characterization and magnetorheological study of magnetorheological (MR) fluids composed of iron particles and sepiolite fibers, used as a thickening agent. The work is aimed at (a) understanding the effect of the sepiolite addition on the MR response; and (b) finding an appropriate formulation allowing a good sedimentation stability keeping a relatively low off-state viscosity and providing an enhanced MR effect. In the presence of an applied magnetic field, the composite MR fluid exhibits a yielding behavior with a progressive enhancement of the field-induced static yield stress with increasing volume fractions of both iron and sepiolite. Such effect is attributed to a friction between gap-spanning aggregates composed of iron particles and sepiolite-oil viscoplastic matrix. The field-induced dynamic yield stress shows an initial increase with the sepiolite concentration (explained by a partial expulsion of the sepiolite fibers from the aggregates) followed by a decrease. The proposed mechanisms are supported by developed qualitative theoretical models, one of which is based on homogenization approach of Château *et al*. J. Rheol. **52**, 489 (2008). From the practical point of view, the formulation containing 10 vol% of iron and 4 vol% of sepiolite seems to combine a perfect sedimentation stability with moderate values of the plastic viscosity and of the off-state static yield stress (only ~5 Pa) and with a relatively important static and dynamic yield stress enhancement (30% and 60%, respectively).

Keywords: Magnetorheological fluids, Magnetorheological effect, Sepiolite, Yield Stress, Homogenization approach

I. Introduction

Magnetorheological fluids (MRFs) belong to a class of smart materials which exhibit sharp and reversible phase transition from a viscous fluid-state to a solid-like state under an

applied external magnetic field [1, 2]. Such fluids consist of magnetizable particles suspended in a nonmagnetic liquid, such as silicone oil, hydrocarbon or aqueous carrier fluid. As an external magnetic field is applied, such particles become magnetized along the magnetic field direction, and can attract each other by strong magnetic dipolar interactions. As a result, fibril-like structures are formed in the medium, thus contributing to a drastic change in the rheological properties of the MRF. In particular, these structures can span the width of a flow channel and bloc the flow. To make the MRF flow through the channel one have to break the structures applying a threshold shear stress, called the yield stress [3]. The yield stress is a key parameter describing magnetorheological (MR) performance of MRF and the magnetic field dependency of the yield stress is referred to as MR effect. MRFs are considered as smart materials and have been experienced a great interest in several engineering applications, such as damping devices, shock absorbers, torque transducers, as well as human muscle stimulators [4-6]. The MR performance of these fluids strongly depends on the magnetic properties, volume fraction, shape, size and morphology of the suspended particles [2].

Among several particles, iron microspheres have been extensively used because they have strong magnetic properties and suitable size for developing a strong MR effect. Nevertheless, iron has a high density as compared to a suspending fluid, resulting in a significant gravitational sedimentation of particles. Several strategies have been adopted to improve the sedimentation stability of MRFs, including incorporation of thickening agents, development of dimorphic MRF or designing appropriate coatings of magnetic particles.

As thickening agents, polymer solutions, small silica nanoparticles or clays can be used. They form a gel network with viscoplastic properties impeding particle settling [7, 8]. Hato *et al*. have used 0.5-3 wt. % of submicron organically modified montmorillonite clay with 25 wt.% (about 4 vol.%) of carbonyl iron particles (CIPs) in silicone oil to decrease the sedimentation, but the shear moduli in the presence of the magnetic field decreased with increase of the clay amount [9]. Other authors used 0.1 wt.% of fibrous clays - halloysite, attapusite and sepiolite, respectively, with 70 wt.% (about 23%) of CIPs in silicone oil [10-12]. These clays allowed better sedimentation stability but the yield stress was reduced by a factor of about two as compared to the fluids without addition of clay. The authors have not focused attention on such a decrease of the MR effect but the reported scanning electron microscopy pictures of the iron-clay composites reveal adsorption of the clay nanoparticles onto the iron microparticle surface. The presence of clay nanoparticles on the iron surface likely impedes a close contact between iron particles under applied magnetic field; this likely decreases magnetic forces between iron particles leading to a decrease of the yield stress.

Lopez-Lopez *et al*. have used 10-40 g/L (about 1.3-5wt.%) bentonite organoclay with 10 vol. % iron particles in kerosene to decrease the sedimentation [13]. As opposed to above cited works, Lopez-Lopez *et al*. report a three times enhancement of the yield stress as compared to the MRF without bentonite at the magnetic field intensity of H=8kA/m. The net MR effect, characterized by the yield stress increment $\Delta\tau_Y = \tau_Y(H) - \tau_Y(0)$ is clearly higher in the presence of clay and cannot be only explained by existence of the yield stress $\tau_Y(0)$ at zero field due to clay network. This clay-induced enhancement of the MR effect has been interpreted in terms of a combined effect of the field-induced iron particle structuring and formation of the clay gel network. Nevertheless, a deep physical interpretation of the clay particles effect (leading to either enhancement or a decrease of the MR effect) is still missing.

Later on, Bombard *et al*. has developed an MRF based on silica covered CIP dispersed in polyalphaoleifin oil/octanol mixed with the ferromagnetic chromium dioxide (CrO_2) and non-magnetic (or rather weakly antiferromagnetic) goethite fiber-like particles to improve the MR effect varying the total concentration of both species up to 45vol% [14]. This composition allowed obtaining a better sedimentation stability thanks to a viscoplastic behavior of the fiber network and a yield stress enhancement by a factor of two-to-three as compared to the suspensions without addition of fibers. This enhancement is explained by nanofiber induced interparticle friction and by local rising in the magnetic permeability between iron spheres mediated by magnetic nanofibers. More recently, Kim *et al*. [15, 16] have tested mixtures of CIP with ferromagnetic CrO_2 nanoparticles dispersed in silicone oil and confirmed a better sedimentation stability and a stronger MR response of their suspensions as compared to the MRFs without CrO_2 addition.

Like MRF stabilized with silica or clay gels, dimorphic MRF are composed of two kinds of particles, at least one of which has a rod-like shape. In dimorphic MRF, rod-like particles usually form a network maintained by friction contacts between particles rather than by attractive colloidal forces. A series of studies has been performed with a mixture of spherical iron microparticles and iron micro- or nanowires. These mixtures exhibited an improved MR response and better sedimentation stability than the suspensions containing only spherical iron particles at the same volume fraction [17-19]. The MR effect enhancement in this case can been interpreted by (a) smaller demagnetizing fields in the rod-like particles allowing a higher magnetization at the same external magnetic field [20]; (b) possible solid friction between rod-like particles [21] and (c) strengthening of the particle structures by the presence of magnetic nanofibers in the contact region between magnetic microspheres [18].

Another solution allowing improvement of the MRF colloidal and sedimentation stability consists in designing special coatings on the magnetic particles' surface increasing the separation between metal oxide surfaces and thus decreasing inter-particle attractive potentials. For instance, Fang *et al*. [22] grafted a conducting polyaniline layer with a multiwall carbon nanotube nest onto the surface of CIP dispersed in silicone oil. Such a thick non-magnetic double layer allowed a considerable improvement of the MRF sedimentation stability at the cost of partial loss of the MR effect likely because of a decrease of magnetic interactions between iron particles. Despite their attractive physical properties, the use of such sophisticated coatings as well as rod-like particles in dimorphic MRFs is limited mostly because of high cost of these coatings and of rod-like particle fabrication.

Suspensions with thickening agents remain cost-effective solution for fabrication of stable MRFs. However, thixotropic behavior and high viscosity and yield stress of the gel network (inherent for all above reported results) present serious drawbacks for smart MR devices. In this paper, we focus on sepiolite clay thickening additive to suspension of iron particles and we are aimed at (a) finding the best formulation allowing a good sedimentation keeping a relatively low off-state viscosity (at zero field) and having an enhanced MR effect; (b) understanding the effect of the sepiolite addition to the MR effect. To this purpose, we perform a systematic magnetorheological study of the suspensions of iron particles dispersed in a silicone oil in the wide range of the iron (5-20 vol%) and sepiolite (1-5 vol%) concentrations.

Sepiolite is a natural microcrystalline-hydrated magnesium silicate, exhibiting a peculiar micro-fibrous morphology constituted by alternating blocks and channels aligned in the direction of the long axis [23, 24]. This needle-like morphology with large aspect ratio (1–10 μm in length and 20–40 nm in diameter) makes this natural mineral clay a very promising additive for magneto- and electrorheological fluids [25, 26].

II. Experimental

A. Materials

Silicone oil (kinematic viscosity 500 cSt at 25 °C and density 0.967 g/cm^3) from Sigma-Aldrich (France); aluminum stearate (AlSt) from Fluka (France); iron (≥99.5%) particles of spherical shape, AnalaR NORMAPUR® analytical reagent, reduced by hydrogen (density 7.86 g/cm^3 and 1-4 μm in diameter as determined by optical microscopy) from Prolabo® VWR International (United States); sepiolite Pangel S9 grade (density 2.362 g/cm^3) from Tolsa (Spain). Deionized water (18.2MΩ×cm) was used for sepiolite treatment.

B. Sepiolite treatment

In natural state, sepiolite fibers form large bundle-like aggregates, thus, it is necessary to disaggregate the fibers, following the protocol suggested in our previous work [26]. Sepiolite was first ultrasonicated for 40 min in water (dispersion at 10 wt.% of sepiolite) using a high power ultrasound tip (Bioblock Scientfic Vibra Cell 75041, 20 kHz and 750 W) working at 210W (28% of maximum amplitude) by pulses of 5 s spaced by 2 s "off" periods. Then the fibers were dried at 100 °C for 12 h.

C. MRF preparation

MRFs were prepared using silicone oil, iron particles, sepiolite fibers and aluminum stearate (AlSt) used for colloidal stabilization of iron particles. AlSt was dispersed in silicone oil at concentration 0.027 mmol/g of iron as suggested in [27]. Then sepiolite was added at vigorous stirring and at different volume fractions (φ_{sep}=1, 2, 3, 4 and 5 vol%) defined as the ratio of the sepiolite volume to the volume of the final suspension, including iron particles, oil, AlSt and sepiolite. Finally, iron powder was added at three different volume fractions of iron (φ = 5, 10 and 20 vol%), defined as the ratio of the iron volume to the volume of the final suspension. MRFs were mechanically stirred at 250 rpm for 6h. Before rheological measurement, all samples were degasified under vacuum for 15 minutes. The prepared samples containing only iron were labeled by S[X], while the samples containing both iron and sepiolite – by S[X:Y], where X and Y are respectively the volume fraction of iron and sepiolite, indicated in vol%. For example, the sample S[10:5] means that it is composed of 10%vol. of iron and 5%vol of sepiolite.

D. Characterization

Scanning electron microscopy (SEM) was carried out on TESCAN VEGA3 scanning electron microscope, operated at an accelerating voltage of 20 kV in backscattered electrons (BSE) detection mode. In addition, SEM with energy-dispersive X-ray spectroscopy (EDX) was carried out using OXFORD Max 50 system. To inspect the MRF microstructure induced by an applied magnetic field, instead of using the silicone oil, we prepared MR elastomers composed of 10 vol% of iron and 5 vol% of sepiolite dispersed in a silicone elastomer RTV 141A/141B (RhodorSil, France) at 10/1 ratio. This MR elastomer was cured at 120°C for 2 h in the presence of the magnetic field of an intensity about H≈30 kA/m. Then the sample was cryo-fractured in a manner that the fracture plane was parallel to the applied magnetic field.

The surfaces of the fractured sample were sputtered with platinum/palladium. In addition to it, Transmission electron microscopy (TEM) was carried out using JEOL 1400 transmission electron microscope, operated at an accelerating voltage of 100 kV. The TEM micrographs of the diluted suspension of iron and sepiolite particles were recorded in the absence of the magnetic field from a very little drop of a liquid suspension, which was deposited on a copper grid of 300 mesh covered by amorphous carbon.

The magnetization measurements of MRFs were performed at room temperature and at different iron and sepiolite concentrations using a vibrating sample magnetometer (VSM 4500) from EG&G Princeton Applied Research (USA). A fluid-like MR sample was inserted into a Teflon cylindrical container with internal dimensions ∅3×10 mm, sealed with a Teflon cover and introduced into the apparatus. Harmonic vibration of the container at a frequency of 82 Hz in the presence of an externally applied magnetic field generated an alternating electromotive force (e.m.f.) in pick-up coils, which was converted to the sample magnetic moment $\mathcal{M}$ (measured in emu) after internal calibration. Knowing the sample mass m, one firstly obtains the mass density of the magnetic moment of the measured sample, $\sigma = \mathcal{M}/m$, in emu/g. The volume density of the magnetic moment or magnetization M in kA/m is then obtained through a simple relationship: $M=\sigma\rho$, where ρ is the MRF density in g/cm^3, whose values are given in Table I for all measured MRF samples. To measure the magnetization of iron particles, the Teflon container was filled with a dry iron powder (as obtained from the supplier) and a similar protocol was applied.

The rheological measurements were carried out using ThermoHaake RheoStress RS600 rotational control stress rheometer. The flow curves (dependencies of the shear stress on the shear rate) were measured in controlled stress mode using the plate-plate geometry with a diameter equal to 35 mm and with surface roughness of 40 μm ensured by gluing a glass paper on both rheometer plates. Most of measurements were conducted with the gap between the two plates fixed to 0.5 mm and the uniform magnetic field was applied by a coil placed coaxially with the rheometer axis.

The protocol used for rheological measurement consisted in three steps: (a) pre-shear at 200 s^{-1} during 60 s in the absence of magnetic field, (b) application of the magnetic field of a desired intensity ranging form H=0 to 30.6 kA/m and waiting period of 30 s with no shear; (c) application of an increasing continuous shear stress ramp from 0 Pa up to a desired value of the maximum stress in the presence of the magnetic field; (d) application of a decreasing step-wise ramp of shear stress with 15 steps, each lasting for 60 s in the presence of the magnetic

field. The data were collected from the decreasing stress ramp (stage (d)) because it gave a much better reproducibility as compared to the increasing stress ramp (stage (c)) for which the threshold stress of the flow onset (static yield stress) depended on initial microstructure of the MRF and therefore might vary from measurement to measurement.

Some rheological measurements were conducted at strong magnetic fields (up to ~480 kA/m) generated by a noncommercial electromagnet described in detail in our previous work [28]. This experimental setup suffered from sample expulsion problem such that only the static yield stress could be safely determined from increasing stress ramp experiments, as the critical stress above which the suspension started to flow.

To realize the sedimentation test MRFs were placed in the transparent polystyrene cuvettes and the pictures were recorded with a photographic camera (Canon-EOS1100D) during 250 h. To extract the evolution of the sediment height with time, the pictures were processed with ImageJ software.

III. Results and discussion

A. Magnetization

The magnetization curves (dependency of the magnetization M on the applied magnetic field H) of MRF containing either only iron particles or iron with sepiolite at 5% volume fraction are plotted in Fig. 1 for three different volume fractions of iron. The magnetization curve of the dry iron powder is shown in the inset of Fig. 1. Since precise microscopic mechanism of magnetization is of a secondary importance for magnetorheology, the magnetization curves were fitted to a simple empirical Fröhlich-Kennelly equation [29]:

$$M = \frac{\chi M_S H}{\chi |H| + M_S}, \qquad (1)$$

with two following adjustable parameters: M_S - the saturation magnetization and χ - the initial magnetic susceptibility. The values of M_S and χ are reported in Table I for different samples including iron particles along with the samples' density and the saturation magnetization values σ_S in emu/g units. All the magnetization curves replotted in emu/g units are presented in Fig. S1 of Supplementary Materials [30]. Firstly, it is noticed that the saturation magnetization of iron AnalaR NORMAPUR® particles ($\sigma_{S,IP}$=230±22 emu/g) is close to the saturation magnetization of the bulk iron ($\sigma_{S,BI}$≈222 emu/g) [31], or, more precisely the known bulk iron value $\sigma_{S,BI}$ fits into the confidence interval of our $\sigma_{S,IP}$ measurement. Secondly, we check that for each MRF sample, the product of the iron magnetization

saturation M_{Fe} by the iron volume fraction φ in the sample falls within experimental errors into the confidence interval of the MRF magnetization saturation (M_S) measurement ($\varphi M_{Fe}=M_S$). Then, it can be observed in Fig. 1 that the magnetization curves of MRFs containing iron with sepiolite seem to overlap with the curves of MRFs containing only iron particles at the same volume fraction of iron. A difference at 10 vol% of iron (between samples S[10] and S[10:5]) seems to fall within the standard deviation of the fit by Eq. (1), as inferred form Table I.

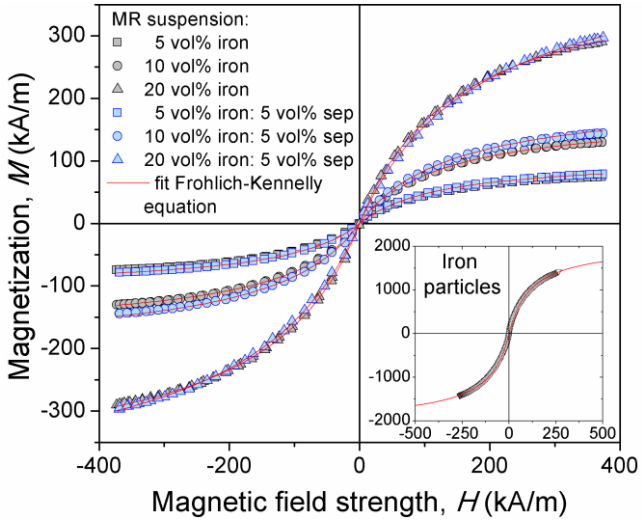

Fig. 1. Magnetization curves (volume density M of the magnetic moment in kA/m versus magnetic field strength H) for different MRFs containing either only iron (S[5], S[10] and S[20]) or iron and sepiolite at 5 vol% (S[5:5], S[10:5] and S[20:5]). Red solid lines stand for the fit of experimental data by the Fröhlich-Kennelly law [Eq. (1)]. The inset shows the magnetization curve of the dry iron powder.

MRF saturation magnetization is expected to be defined only by the saturation magnetization of constitutive iron particles and on their volume fraction and to be independent of the suspension microstructure (spatial distribution of particles, local gaps between particles in aggregates, etc.). Thus, the presence or absence of sepiolite should not alter magnetization saturation at the same iron volume fraction, which is confirmed by our measurements [see Table I]. On the other hand, the initial magnetic susceptibility (defined by the slope at the origin of the magnetization curve) usually strongly depends on the suspension microstructure. For example, structured MRF with dense aggregates of closely spaced iron particles give much higher magnetic susceptibility as compared to an unstructured MRF [32]. Our MRFs experience a strong structuring both in the presence and in the absence of sepiolite [cf. Fig. 2]. Thus, the presence of sepiolite in the gaps between iron particles inside the structures would increase an effective separation between particles and would lead to a decrease of magnetic interaction energy between them and, consequently, to a decrease of the

magnetic susceptibility. Numerical simulations show that an increase of the separation between iron particles by a few nanometers induces a several dozen percent decrease in initial magnetic susceptibility [33]. Near similar values of χ for the suspensions with and without sepiolite indicates that the sepiolite fibers or flocs are likely fully squeezed out from the gaps between iron particles in the aggregates, such that the aggregate morphology remains intact by the presence of sepiolite.

Table I: Density and magnetic properties of iron particles and MRFs

Samples	**Code**	**Density (g/cm^3)**	σ_s **(emu/g)**	M_s **(kA/m)**	χ
Iron particles	N/A	7.86	230±22	1810±170	17.7±0.6
5% iron	S[5]	1.311	68.3±6.8	90±9	0.80±0.07
10% iron	S[10]	1.646	95.8±13.6	158±22	1.37±0.11
20% iron	S[20]	2.346	157±15	369±34	2.70±0.21
5% iron, 5% sepiolite	S[5:5]	1.380	68.2±6.5	94±9	0.86±0.07
10% iron, 5% sepiolite	S[10:5]	1.721	107±15	184±25	1.44±0.11
20% iron, 5% sepiolite	S[20:5]	2.415	167±15	404±36	2.38±0.21

B. Microstructure

To get a deeper insight into the MRF microstructure we have performed TEM and SEM-EDX analyses shown in Fig. 2. TEM images were collected on the diluted liquid suspension of iron and sepiolite dispersed in the silicone oil in the absence of the magnetic field. The TEM micrograph in Fig. 2a shows that sepiolite fibers are likely gathered into flocs of a characteristic size of a few microns and that the flocs seem to be homogeneously distributed around iron particles. Such aggregation of fibers should come from colloidal van der Waals interactions between them. To inspect the microstructure under applied magnetic field, SEM images were recorded on the silicone MR elastomer containing 10 vol% of iron and 5 vol% of sepiolite and cured in the presence of the magnetic field, as described in Sec. II-D. SEM micrographs in Fig. 2b and c show that iron particles gather into long aggregates aligned with the magnetic field (applied during elastomer curing) and having a length larger than 100 μm and a thickness of about 10 μm corresponding to a few particle diameters. Such relatively thick MR structures are typically observed in MRFs at particle volume fractions above a few volume percent [34] and are more energetically favorable than single chains [35].

Furthermore, at a higher magnification of the SEM image (Fig. 2f), one can observe a quite heterogeneous spatial distribution of iron particle chains with the inter-chain distance varying between ~10 µm (as in Fig. 2b) and ~300 µm. Sepiolite fibers are invisible in SEM pictures because of a poor difference in electron density in sepiolite and silicone matrix atoms but can be easily detected by the EDX analysis, detecting the presence of iron belonging to iron particles [Fig. 2d] or magnesium belonging to sepiolite [Fig. 2e]. Comparing Figs. 2c, 2d and 2e, we see that sepiolite is uniformly distributed around the aggregate of iron particles, a weaker intensity of magnesium signal in the location of the iron aggregate indicates a smaller content of sepiolite within the aggregate. Even though it is impossible to quantify the sepiolite amount within the aggregate, the observation in Fig. 2e at least does not contradict to the hypothesis (supported by magnetization measurements, cf. Sec. III-A) that sepiolite could be partially expulsed from the aggregates.

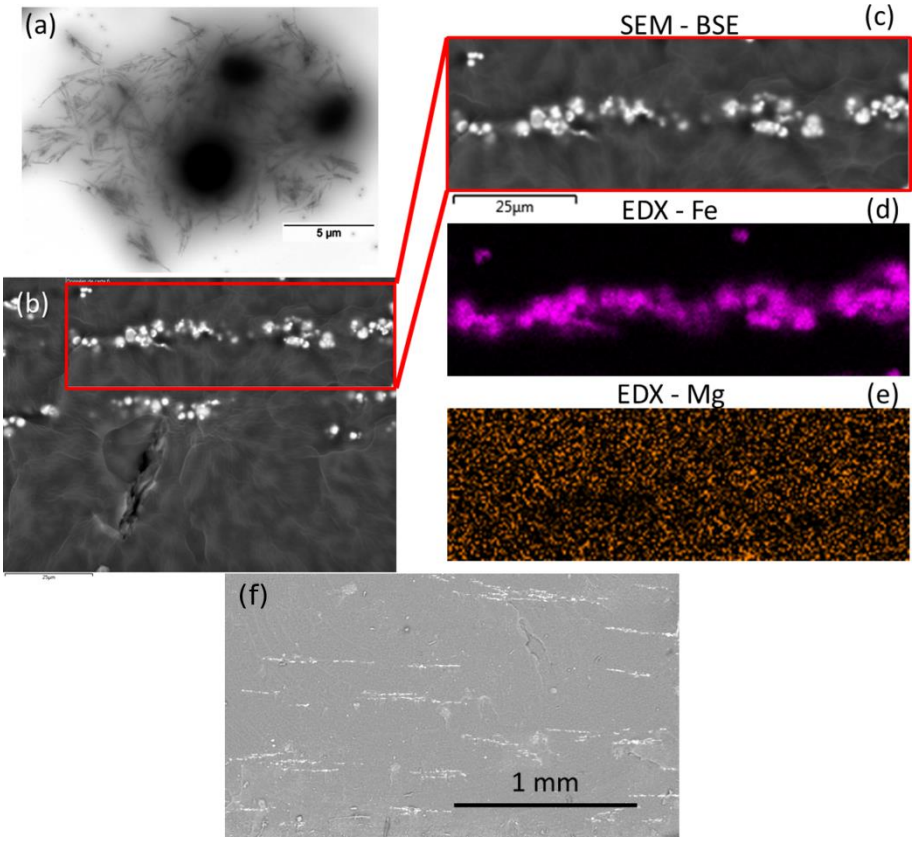

Fig. 2. TEM micrograph of the liquid MRF containing iron and sepiolite dispersed in the silicone oil (a); SEM image of a cross-section of silicone MR elastomer cured in the presence of a magnetic field and containing 5vol% of sepiolite and 10 vol% of iron at different magnifications (b, c and f); SEM-EDX image analyzing the presence of iron (d) or magnesium (e). Scale bar in (a) is 5 µm.

C. Sedimentation behavior

To inspect the effect of the sepiolite addition on MRF sedimentation behavior in the absence of the magnetic field, we have recorded the sedimentation process during 240 h (10 days) and estimated at each moment of time t the relative sediment height defined as the ratio h/h_0 (expressed in percent) of the sediment height $h(t)$ to the initial height h_0 of the MRF column. The time dependency of the relative sediment height is shown in Figs. 3a, b and c for MRFs containing, respectively, 5, 10 and 20 vol% of iron and 0, 1 or 4 vol% of sepiolite, while representative pictures of the sedimentation experiment are shown in Fig. 3d. All the curves show an initial near linear decrease of h/h_0 with time followed by a final plateau at long times. From these curves, the two following sedimentation parameters are extracted: (a) the final relative sediment height h_f/h_0 – the plateau value of h/h_0, and (b) the characteristic sedimentation time, t_s, defined at the intercept of the tangent line at the origin with the final plateau, as shown in Fig. 3a. These values are summarized in Table II. As expected, a relatively strong sedimentation is observed for all MRFs without sepiolite addition with the final relative sediment height going from 27 to 66 % when increasing iron concentration from 5 to 20 vol%. The sedimentation is considerably reduced and slowed down when 1 vol% of sepiolite is added, however the final relative sediment height is still far from 100% such that the particles still settle considerably during a period on the order of a few days without shaking; this is undesirable for MR commercial devices. When the sepiolite amount is increased to 4 vol%, the sedimentation almost disappear in the samples containing 10 and 20vol% of iron particles, while it is still visible (h_f/h_0=90%) at 5 vol% of iron. The general trend of increasing sedimentation stability and slowing down the sedimentation process at increasing iron or sepiolite concentration is explained by an increased viscous dissipation in the suspending fluid with increasing concentration of both species, as well as by formation of stronger gel network of sepiolite clay at increasing sepiolite amount. For a deeper understanding of the concentration effect, we have to inspect the rheological behavior of the suspending fluid of our MRFs (sepiolite- silicone oil mixture) and the rheological response of the MRFs in the absence of magnetic field (hereinafter referred to as off-state response).

Table II. Relative sediment height and characteristic sedimentation time of MRFs at different iron and sepiolite amounts. N/A corresponds to impossibility to find the sedimentation time at the values h_f/h_0 close or equal to 100%.

sepiolite / iron	0		1 vol%		4 vol%	
	h_f/h_0 (%)	t_s (h)	h_f/h_0 (%)	t_s (h)	h_f/h_0 (%)	t_s (h)
5 vol%	27	9	71	61	90	110
10 vol%	29	22	50	31	97	N/A
20 vol%	66	71	76	106	100	N/A

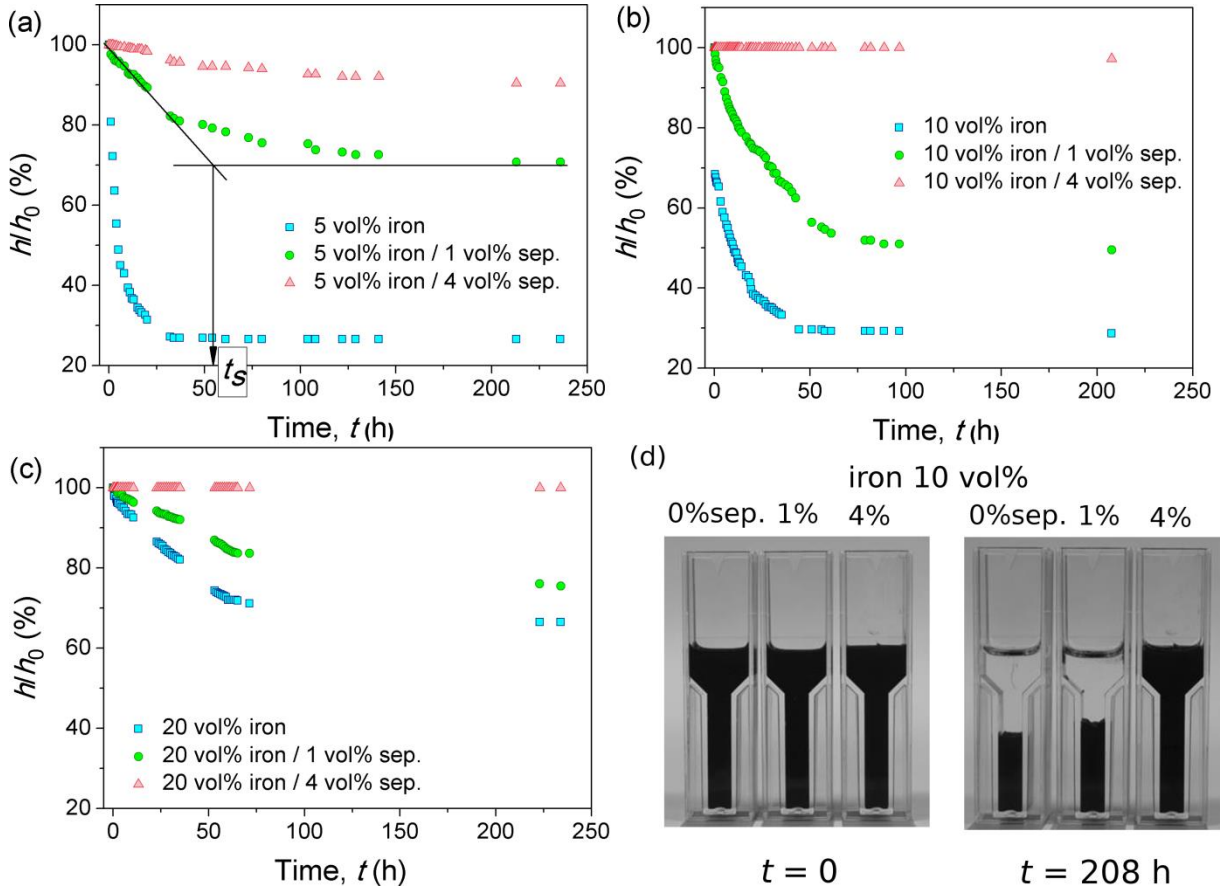

Fig. 3. Sedimentation profile as a function of time for the MRFs with different iron concentrations: 5vol% (a), 10 vol% (b) and 20 vol% (c) at different sepiolite concentrations. Images of settling experiments for iron concentration 10 vol% at different sepiolite concentrations and at two values of the elapsed time (t=0 and 208 h) are shown in (d).

D. Off-state rheological response

The flow curves of the suspensions of sepiolite dispersed at different volume fractions in silicone oil without AlSt additive are shown Fig. 4 in linear scale, while they are represented in double logarithmic scale in Fig. S2 [30]. At sepiolite concentration equal to 1

vol%, the suspension shows a Newtonian behavior with a viscosity 20% larger than the silicone oil viscosity (0.485 Pa s). At increasing sepiolite concentration the flow curves are shifted upwards meaning an increasing viscous dissipation and sepiolite suspensions show a shear thinning behavior likely coming from (a) formation of fiber flocs (as revealed in TEM picture of Fig. 2a) because of attractive colloidal interactions between them, and (b) progressive destruction of the flocs with increasing shear rate resulting in a viscosity decrease, as suggested by many authors [36-38]. The off-state flow curves of the MRFs containing both iron and sepiolite particles have a similar shape to those shown in Fig. 4 for oil-sepiolite mixtures and some of them are presented below in Fig. 6. At shear rates $\dot{\gamma}$ >25 s^{-1}, all the flow curves (for oil-sepiolite and MRFs at zero field) are satisfactorily fitted by a linear Bingham rheological equation (red lines in Fig. 4) [39]:

$$\tau = \eta_p \dot{\gamma} + \tau_D , \qquad (2)$$

where two adjustable parameters η_p and τ_D are, respectively the plastic viscosity and the dynamic yield stress, defined as an intercept of the Bingham fit extrapolation with the ordinate axis.

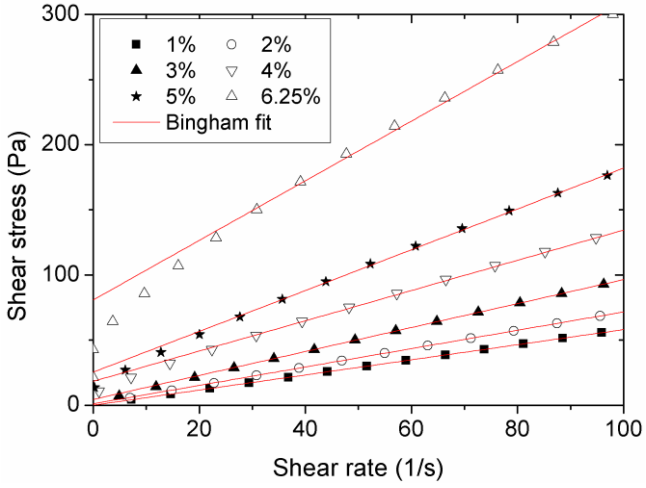

Fig. 4. Flow curves of suspensions of sepiolite fibers dispersed in silicone oil for different sepiolite concentrations volume fractions.

Since at least one of the sizes of sepiolite fibers (diameter of 20-40 nm) is much less than the diameter of iron particles (1-4 μm), at the first approximation, the sepiolite-oil mixture filling the space between iron particles can be considered as a continuous medium. For such ideal scale separation, the volume fraction of sepiolite $\varphi_{sep}' = \varphi_{sep}/(1-\varphi)$ in the suspending liquid is a more pertinent parameter than the volume fraction φ_{sep} of sepiolite in the whole MRF because the former allows a correct comparison between MRFs containing

different volume fractions φ of iron particles. The dependencies of off-state plastic viscosity and off-state yield stress on the sepiolite concentration φ_{sep}' are shown in Figs. 5a and 5b respectively for suspensions of different content of iron including 0 vol% corresponding to oil-sepiolite mixtures. For all iron concentrations, both the plastic viscosity and the yield stress are strongly increasing functions of sepiolite concentration, which is explained by the fact that the gel network of sepiolite fibers gets stronger with increasing concentration because the number of contacts between sepiolite fibers per unit volume increases at least as a square of the volume fraction of sepiolite fibers. In particular, the dynamic yield stress of the sepiolite-oil mixture follows a power-law trend, $\tau_D \sim \varphi_{sep}^{3.7}$ with the exponent fitting to the range 2-5 provided by numerous experiments and models on flocculated fiber suspensions [40-43]. Progressive addition of iron particles to the suspending sepiolite-oil mixture leads to an increase of the energy dissipation resulting in higher plastic viscosity and dynamic yield stress with increasing iron concentration φ, as manifested by an upward shift of $\eta_p(\varphi_{sep}')$ and $\tau_D(\varphi_{sep}')$ curves in Figs. 5a and 5b. Such effects in Bingham suspending fluids can be modelled by the homogenization approach of Château *et al.*, in which the suspending fluid viscosity is calculated at appropriately defined local shear rate [44]. It gives the following expressions for the off-state plastic viscosity $\eta_p(\varphi_{sep}', \varphi)$ and off-state dynamic yield stress $\tau_D(\varphi_{sep}', \varphi)$ of the MRF as function of the iron particle concentration φ and of the plastic viscosity $\eta_p(\varphi_{sep}', 0)$ and the yield stress $\tau_D(\varphi_{sep}', 0)$ of the suspending sepiolite-oil mixture [45]:

$$\eta_p(\varphi_{sep}', \varphi) = \eta_p(\varphi_{sep}', 0) g(\varphi) \tag{3-a}$$

$$\tau_D(\varphi_{sep}', \varphi) = \tau_D(\varphi_{sep}', 0) \sqrt{g(\varphi)(1-\varphi)}, \tag{3-b}$$

where $g(\varphi) = \eta(0, \varphi)/\eta_0$ is the relative viscosity of the suspension of iron particles dispersed in a Newtonian solvent of a viscosity η_0 (silicone oil without sepiolite in our case). The magnitude $g(\varphi)$ was taken from the measurement of the off-state viscosity $\eta(0, \varphi)$ of MRFs without sepiolite addition and was fitted by the Maron-Pierce equation [46], $g(\varphi) = (1-\varphi/\varphi_m)^{-2}$, with an adjustable parameter $\varphi_m = 0.5$ having the meaning of the maximum packing fraction of spherical iron particles. For calculations of the theoretical dependencies $\eta_p(\varphi_{sep}', \varphi)$ and $\tau_D(\varphi_{sep}', \varphi)$, we have used experimental values of the magnitudes $\eta_p(\varphi_{sep}', 0)$ and $\tau_D(\varphi_{sep}', 0)$, which were fitted by respectively a fourth-order

polynomial and power-law functions. These fits are shown by red dashed lines in Figs. 5a and 5b.

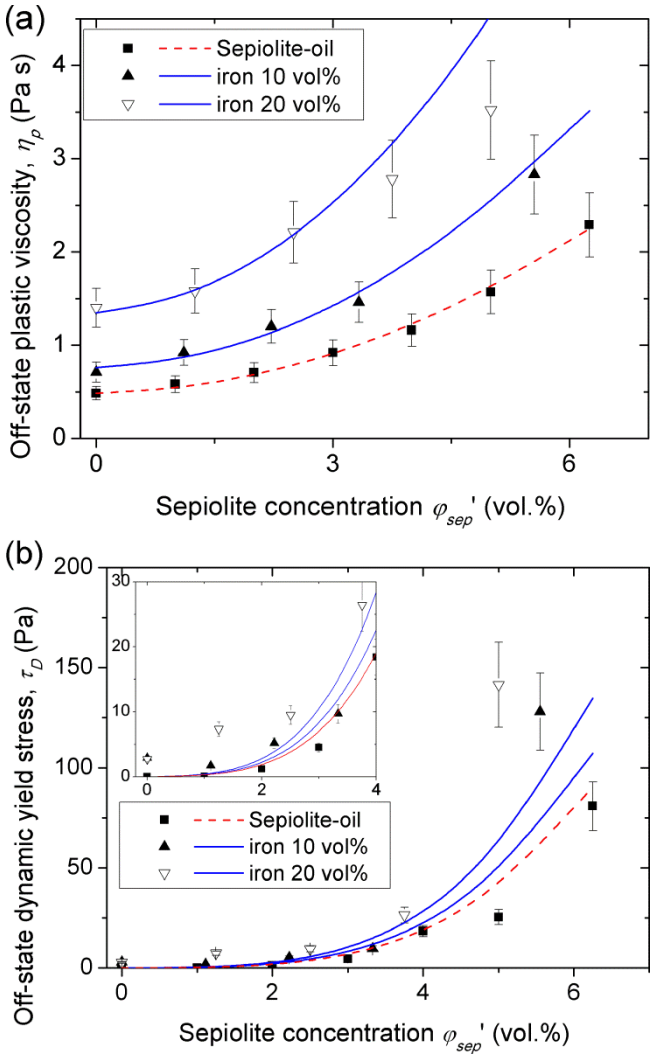

Fig. 5. Off-state plastic viscosity (a) and off-state dynamic yield stress (b) of MRFs as a function sepiolite concentration φ_{sep}' for different concentrations of iron including 0 vol% corresponding to the suspending fluid (sepiolite-oil mixture). Symbols correspond to experimental data, red dashed lines – to the fit of $\eta_p(\varphi_{sep}',0)$ and $\tau_D(\varphi_{sep}',0)$ dependencies by polynomial and power-law functions respectively, blue solid lines – to theoretical dependencies [Eqs. (3-a) and (3-b)].

Theoretical dependencies $\eta_p(\varphi_{sep}',\varphi)$ [Eqs. (3-a)] and $\tau_D(\varphi_{sep}',\varphi)$ [Eq. (3-b)] of the off-state plastic viscosity and off-state dynamic yield stress on the sepiolite concentration φ_{sep}' are shown by solid blue lines on Figs. 5a and 5b, respectively. There is a much better agreement between theory and experiment for the plastic viscosity [Fig. 5a] than for the dynamic yield stress [Fig. 5b]. Homogenization approach seems to considerably underestimate the off-state dynamic yield stress, still providing a correct qualitative effect of

the yield stress increase with increasing volume fraction of iron particles. The quantitative discrepancy is larger for larger volume fractions of both sepiolite and iron and likely indicates that the scale separation approach is no longer valid at high concentrations of both species. The sepiolite fiber flocs are expected to increase in size with increasing sepiolite concentration. Above some value of φ_{sep}', the floc size likely becomes comparable with the size of iron particles such that, strictly speaking, the sepiolite-oil mixture cannot be longer considered as a continuous medium for iron particles but one have to consider iron particles and sepiolite flocs as two equitable components dispersed in a silicone oil. It is however more difficult to handle this second approach because we do not have enough information on the morphology, shape and size of the fiber flocs under flow.

Finally, better sedimentation stability with increasing concentration of both sepiolite and iron (as discussed in Sec. III-C, Fig. 3) perfectly correlates with a strong increase of the off-state plastic viscosity and dynamic yield stress with increasing concentration of both species.

E. Magnetorheology

We can now inspect the MR effect of our MRFs as a function of the sepiolite concentration. Figure 6 shows the flow curves of MRFs containing 5, 10 and 20 vol% of iron and 0, 3 and 4 or 5 vol% of sepiolite for each concentration of iron in the presence of the applied magnetic field of an intensity H ranging between 0 and 30.6 kA/m. At shear rates $\dot{\gamma}$ >25 s^{-1}, all the flow curves were fitted to Bingham rheological law [Eq. (2)] and the two adjustable parameters – the dynamic yield stress τ_D and the plastic viscosity η_p were determined for each curve. Another important parameter – the static yield stress τ_S – was determined as the stress value at low shear plateau of the flow curves plotted in double logarithmic scale (see arrows in Fig. S3 in Supplementary Materials [30]), as suggested in [47]. The measurements at strong magnetic fields (H≈100-480 kA/m) were carried out at increasing stress ramp; in those experiments, the static yield stress corresponded to the threshold stress required for the flow onset. The measurements at low magnetic fields (H=0-30.6 kA/m) were carried out at a decreasing stress ramp, and the yield stress stands for the threshold stress required to stop the flow.

Let us first inspect rheological behavior of MRF without sepiolite addition (left column on Fig. 6). The off-state flow curves (at zero applied magnetic field) show a weak Bingham behavior with relatively small dynamic yield stress τ_D≈2-3 Pa at φ=10 and 20vol %

arising likely because of small remnant magnetization of iron particles. When the magnetic field is applied, the flow curves are shifted upwards with increasing magnetic field meaning stronger energy dissipation thanks to appearance of the field-induced structures whose size and therefore hydrodynamic resistance increase with the magnetic field. The flow curves have a rounded shape at shear rates $\dot{\gamma}$ <25 s^{-1} followed by a liner section at $\dot{\gamma}$ >25 s^{-1}. Such a shape can, among other reasons, be caused by a transition from gap-spanning field-induced aggregates composed of iron particles (at $\dot{\gamma}$ <25 s^{-1}) to shorter free aggregates (at $\dot{\gamma}$ >25 s^{-1}) no longer touching the rheometer walls [48]. It is noticeable that linear parts of the flow curves in the absence of sepiolite are almost all parallel to each other indicating that the plastic viscosity (slope of the curve) is nearly independent of the magnetic field intensity, as often observed in the magnetorheology [3].

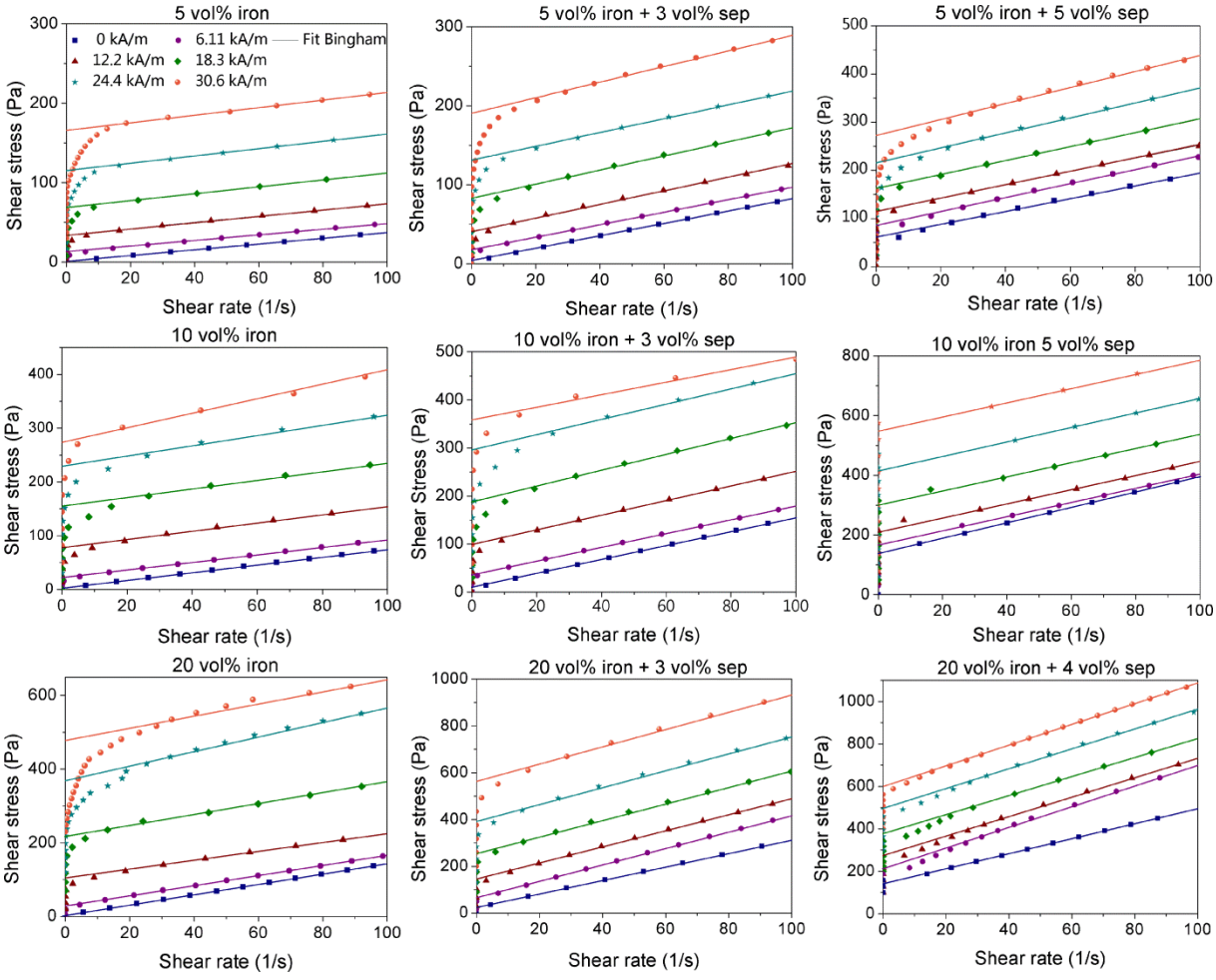

Fig. 6. Experimental flow curves for the MRFs containing 5, 10 and 20 vol% of iron and at the sepiolite concentration φ_{sep}=3, 4 or 5 vol% and for different values of the external magnetic field. Symbols stand for experiments, solid straight lines correspond to the Bingham fit at shear rates $\dot{\gamma}$ >25 s^{-1}.

The flow curves of MRFs with sepiolite addition (middle and right column on Fig. 6) have a shape qualitatively similar to that of the MRFs without sepiolite (left column on Fig.

6). Quantitatively, the off-state flow curves exhibit a noticeable Bingham behavior with a dynamic yield stress achieving a value of about 150 Pa for 5vol% sepiolite concentration. As explained above, such relatively strong off-state yield stress comes from a formation of gel network in the sepiolite-oil mixture. We also remark an increase of the slope of the flow curves (plastic viscosity) with an increase of the magnetic field form 0 to 6.11 kA/m for the MRFs containing 20vol% of iron and 3 or 5vol% of sepiolite (two right graphs in a bottom row of Fig. 6). It is noticeable that the plastic viscosity remains nearly constant in the considered field range (6.11-30.6 kA/m) and larger than that at zero field. Such increase of the plastic viscosity is an atypical behavior for magnetorheology and can be tentatively explained by a partial expulsion of sepiolite fibers or flocs from the field-induces aggregates composed of iron particles. In this case, effective concentration of sepiolite in the space between aggregates increases which results in an increase of the viscosity of the suspending fluid (sepiolite-oil mixture).

Let us now inspect the effect of the magnetic field and of sepiolite addition on the yield stress. The full panel of the experimental dependencies of the static yield stress and dynamic yield stress on the applied magnetic field and on the sepiolite concentration are shown in Supplementary Material [30] (Figs. S4 – S10). MR effect is better represented by the yield stress increment (defined as the difference of the yield stress in the presence and in the absence of the magnetic field). Experimental dependencies of the static and dynamic yield stress increments (respectively, $\Delta\tau_S = \tau_S(H,\varphi_{sep},\varphi) - \tau_S(0,\varphi_{sep},\varphi)$ and $\Delta\tau_D = \tau_D(H,\varphi_{sep},\varphi) - \tau_D(0,\varphi_{sep},\varphi)$) on the applied magnetic field H and on the sepiolite concentration φ_{sep} are shown, respectively, on the left and right columns of Fig. 7 for the iron concentration $\varphi = 10$ vol%. The field dependencies of $\Delta\tau_S$ have qualitatively similar features to those for $\Delta\tau_D$ and both have been fitted by a power-law function, $\Delta\tau_{S,D} \propto H^n$ with an exponent varying in the range n = 1.45 – 1.77 for all experimental $\Delta\tau_S(H)$ and $\Delta\tau_D(H)$ - dependencies at the applied magnetic fields $H \leq 30.6$ kA/m. The power-law fit is shown by solid red curves for the lower and the upper curves of Figs. 7a, c. The found range n = 1.45 – 1.77 of the power-law exponent covers typical values reported for the similar magnetic field range [3] and deviates from the quadratic behavior $\Delta\tau_{S,D} \propto H^2$ predicted for magnetic particles with linear magnetization and relatively low magnetic permeability. Smaller values of n in our experiments are explained by non-linear magnetization of iron particles [cf. inset

of Fig. 1] manifested by a strongly decreasing magnetic permeability with increasing magnetic field.

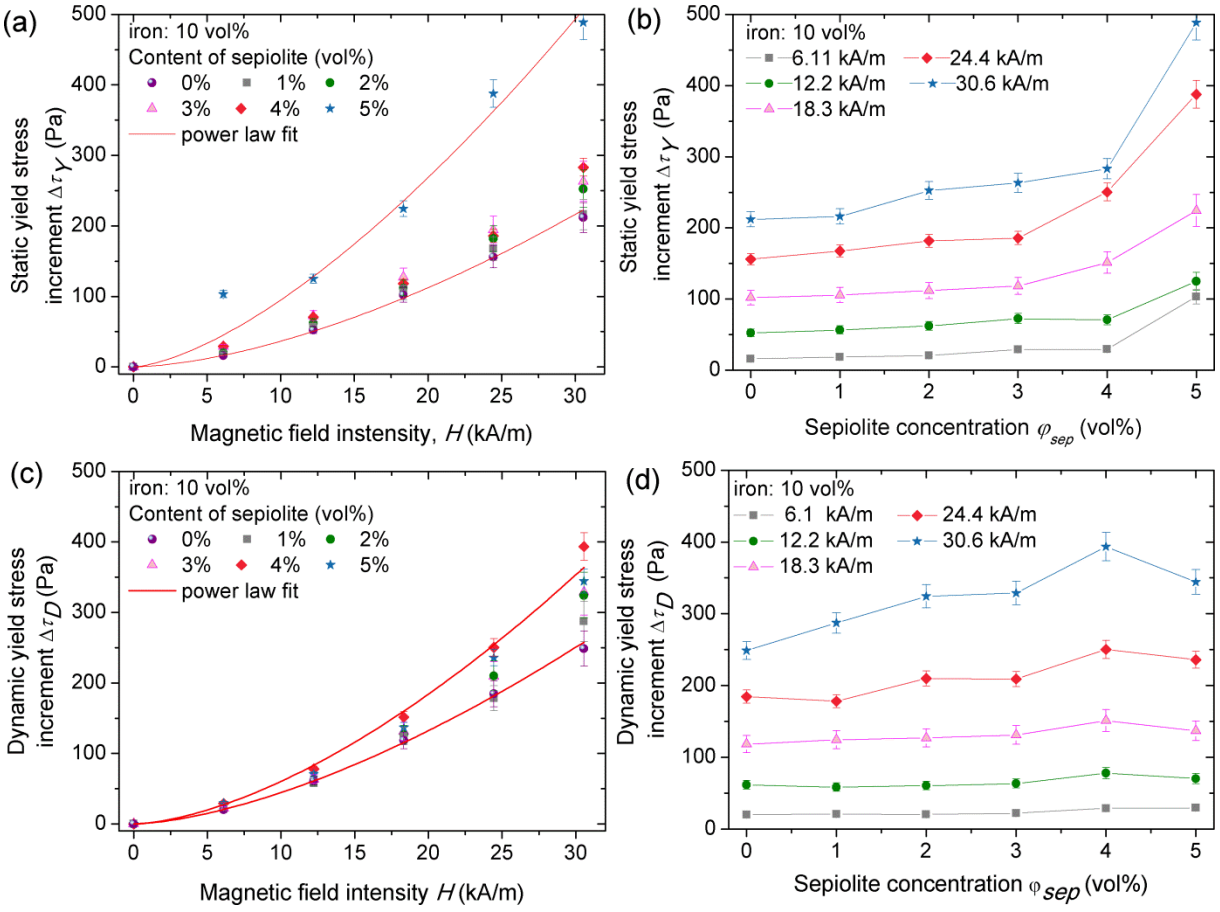

Fig. 7. Static yield stress increment (a, b) and dynamic yield stress increment (c, d) as function of the applied magnetic field (a, c) and as function of the sepiolite concentration φ_{sep} (b, d). The concentration of iron is φ=10 vol%. Solid lines in (a) and (c) correspond to the power law fit; solid lines in (b) and (d) are guides to the eye.

Right column of Fig. 7 shows dependencies of the static and dynamic yield stress increments on the sepiolite concentration. We remark a distinguishable increase of the static yield stress increment $\Delta\tau_S$ with the sepiolite concentration [Fig. 7b], while the effect on the dynamic yield stress increment $\Delta\tau_D$ seems not to be easily distinguishable from experimental errors, except for intermediate magnetic fields, H=24.4 and 30.6 kA/m. Notice that at higher magnetic fields (100<H<480 kA/m), $\Delta\tau_S(H)$ dependencies seem to be qualitatively similar to those at low magnetic fields (Fig. S10 [30] versus Fig. 7a), while $\Delta\tau_S(\varphi_{sep})$ dependencies exhibit a less pronounced increase with φ_{sep} at higher fields (Fig. S10 [30] versus Fig. 7b).

To better appreciate the influence of the sepiolite addition on the MR effect, we introduce an enhancement parameter expressed in percent and defined as the ratio of the

difference of the yield stress increments $\Delta\tau_{S,D}(H,\varphi_{sep},\varphi)$ and $\Delta\tau_{S,D}(H,0,\varphi)$ taken, respectively at given sepiolite concentration φ_{sep} and at zero sepiolite concentration, to the yield stress increment at zero sepiolite concentration. We will distinguish a static yield stress enhancement parameter (A_S) from the dynamic one (A_D) related respectively to $\Delta\tau_S$ and $\Delta\tau_D$:

$$A_S = \frac{\Delta\tau_S(H,\varphi_{sep},\varphi) - \Delta\tau_S(H,0,\varphi)}{\Delta\tau_S(H,0,\varphi)}, \tag{4a}$$

$$A_D = \frac{\Delta\tau_D(H,\varphi_{sep},\varphi) - \Delta\tau_D(H,0,\varphi)}{\Delta\tau_D(H,0,\varphi)}. \tag{4b}$$

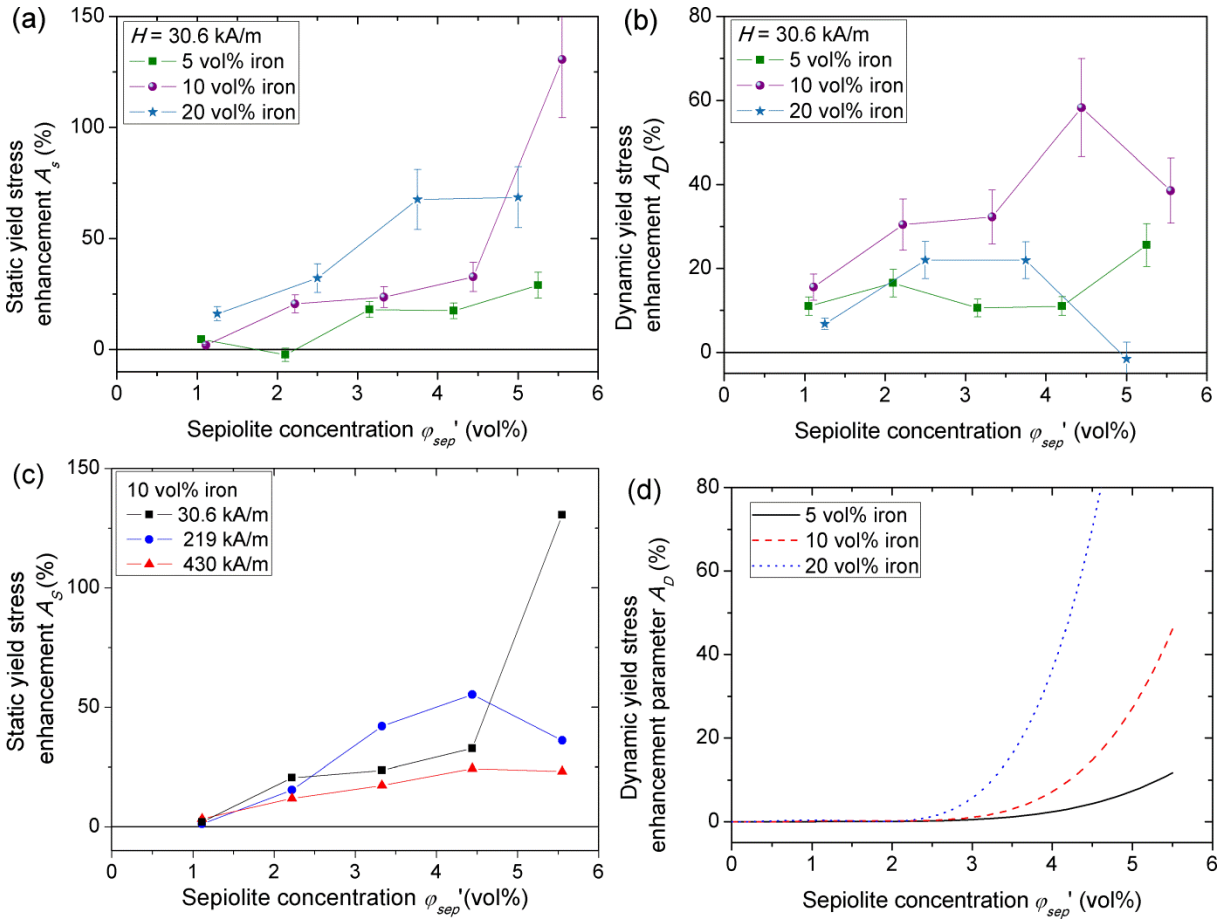

Fig. 8. Experimental dependences of the enhancement parameters A_S (a) and A_D (b) on the sepiolite concentration φ_{sep}' for different concentrations φ of iron particles and at the applied magnetic field H=30.6 kA/m. Experimental dependency $A_S(\varphi_{sep}')$ for different values of the applied magnetic field at the iron concentration φ=10 vol% are shown in (c). The figure (d) shows a theoretical estimation of the upper bound of the parameter A_D as function of sepiolite concentration.

Experimental dependencies of the static and dynamic yield stress enhancement parameters on the sepiolite concentration are shown in Figs. 8a and 8b, respectively for the magnetic field intensity H=30.6 kA/m. In order to compare the curves for different content of

iron particles, the graphs are plotted as function of the sepiolite concentration φ_{sep}' in the suspending fluid (sepiolite-oil mixture). The dynamic yield stress shows a non-monotonic dependence of the parameter A_D on the sepiolite concentration, while the parameter A_S seems to gradually increase with φ_{sep}'. Furthermore, the highest enhancement parameter A_D is obtained at intermediate iron concentration φ=10 vol%, while the highest parameter A_S is obtained for the largest used amount of iron, φ=20 vol%.

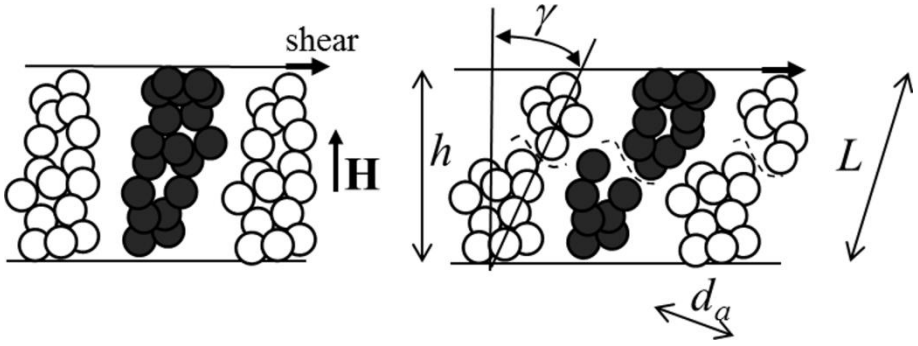

Fig.9. Sketch of the rupture of gap-spanning aggregates at some critical shear strain γ. If the suspending fluid is viscoplastic, a friction between the aggregates and the suspending fluid is expected to contribute to the total shear stress

Different explanations could be given to explain these behaviors. Let us first focus on the static yield stress enhancement. The static yield stress is governed by static gap-spanning particles structures. Thus, the enhancement of the static yield stress increment is unlikely to be attributed to strengthening of the iron particle structures by incorporation of clay particles, as suggested by Lopez-Lopez *et al*. [13] or by an enhanced solid friction between iron particles and sepiolite rods, as suggested by Bombard *et al*. [14] because (a) sepiolite particles introduced in the gaps between iron particles would increase these gaps and decrease the magnetic forces between iron particles; (b) the presence of sepiolite on the surface of iron particles within the aggregates would imply a considerable change in the MRF magnetic susceptibility (as explained in detail in Sec. III-A) that is not the case in our experiments [Fig. 1]. We propose the following macroscopic mechanism as a tentative explanation of the enhancement of the static yield stress increment by sepiolite addition. The static yield stress is often modeled as a maximum of the shear stress versus shear strain dependency when the gap-spanning aggregates are tilted by the applied strain and break at a maximum point [3], as illustrated schematically on Fig. 9. If the suspending fluid possesses a static yield stress, it likely impedes the extension of aggregates when they are tilted by strain producing an effect equivalent to a static friction between aggregates and suspending fluid. Of course, this effect can only appear if there is a relative displacement of the aggregate lateral surface with respect

to the suspending fluid – so called non-affine deformation appearing as a result of either possible wavy or zigzag shape of the aggregates [49] or microscopic rearrangement of the particles inside the aggregates, as predicted by particle level simulations [50]. The friction force exerted on an elementary surface of the aggregate along the longitudinal *z* axis of the aggregate is $dF = \tau_{S0}\pi d_a dz$, where $\tau_{S0} = \tau_S(\varphi_{sep}', 0)$ is the suspending fluid static yield stress and d_a is the aggregate diameter. The total static yield stress of the MRF is expected to be a sum of the magnetic contribution, $\tau_{Sm}(H,\varphi)$ coming from attractive interactions between iron particles and a friction contribution given by the following expression:

$$\tau_{Sf}(\varphi_{sep}') = n_g \int (u - u_0) dF \sim \frac{4\Phi_g}{\pi {d_a}^2 L} \varepsilon \tau_{S0} \pi d_a 2 \int_0^{L/2} z dz \sim \Phi_g \varepsilon \tau_{S0} \frac{L}{d_a}, \qquad (5)$$

where n_g, and Φ_g are respectively the number of gap-spanning aggregates by unit MRF volume and the volume fraction of these aggregates; $u - u_0 \sim \varepsilon z$ is the difference of the absolute values of the displacement vectors of the aggregate and of the suspending fluid, respectively, both at a position *z*; $\varepsilon = (1+\gamma^2)^{1/2} - 1$ and γ are respectively the tensile and the shear strain, *L* is the length of the tilted aggregates and it is on the order of magnitude of the rheometer gap width *h* [Fig. 9]. Note that in an unlike case of affine deformation, we get $u - u_0 = 0$, which results in a zero friction contribution to the static yield stress, $\tau_{Sf} = 0$.

The static yield stress increment in the presence of the sepiolite is therefore given by: $\Delta\tau_S(H, \varphi_{sep}', \varphi) = \tau_{Sm}(H,\varphi) + \tau_{Sf}(\varphi_{sep}', \varphi) - \tau_S(0, \varphi_{sep}', \varphi)$, while in the absence of sepiolite it is approximately equal to the magnetic contribution: $\Delta\tau_S(H, 0, \varphi) \approx \tau_{Sm}(H,\varphi)$. Replacing these magnitudes in the definition of the enhancement parameter [Eq. (4a)], we get the following expression for A_S:

$$A_S = \frac{\tau_{Sf}(\varphi_{sep}', \varphi) - \tau_S(0, \varphi_{sep}', \varphi)}{\tau_m(H,\varphi)} \sim \frac{\Phi_g \varepsilon \tau_{S0} L / d_a - \tau_S(0, \varphi_{sep}', \varphi)}{\tau_m(H,\varphi)} \qquad (6)$$

The first term in the numerator of Eq. (6) is expected to be much larger than τ_{S0} since the aggregate length $L \sim h$ is expected to be much larger than its thickness d_a, while the second term is on the order of magnitude of τ_{S0}. Therefore the difference is expected to be positive. Equation (6) shows that the enhancement parameter A_S is expected to be a growing function of sepiolite concentration that is qualitatively confirmed in our experiments [cf. Fig. 8a]. The effect of the magnetic field is less evident to assess because, on the one hand, the denominator of Eq. (6) increases with the magnetic field and, on the other hand, the volume fraction Φ_g of

gap spanning aggregates increases with the magnetic field giving rise to an increase of the numerator of Eq. (6). Thus, plotting on Fig. 8c $A_S(\varphi_{sep}')$ experimental dependencies for the fixed iron concentration φ=10 vol.% but at different magnetic fields, we observe a non-monotonic trend of the enhancement parameter A_S versus the applied field *H*. The effect of sepiolite concentration can be further enhanced if there is a partial expulsion of sepiolite from aggregates composed of iron particles, which enhances the static yield stress τ_{S0} of the suspending sepiolite-oil mixture between the aggregates. The quantitative comparison of theoretical and experimental $A_S(\varphi_{sep}')$-dependencies is unfortunately impossible since we have a lot of unknown parameters describing the iron aggregates, such as Φ_g, d_a, ε.

Let us now consider the dynamic yield stress enhancement. As commonly admitted, the dynamic yield stress comes from viscous energy dissipation on field-induced aggregates whose size is governed by a balance of cohesive magnetic and tensile hydrodynamic forces [7, 51]. Similarly to the static yield stress, because of the reasons explained above, the dynamic yield stress is unlikely to be enhanced by strengthening of particle aggregates by sepiolite particles or solid friction between iron particles with adsorbed sepiolite fibers on their surface. One could expect a nonzero effect of sepiolite addition on the enhancement parameter A_D if the yield stress additivity rule would not be valid meaning that the total dynamic yield stress is not equal to the sum of the magnetic contribution $\tau_{Dm}(H,\varphi)$ and of the off-state yield stress $\tau_D(0,\varphi_{sep}',\varphi)$. However, adapting the homogenization approach [44] to the flowing MRF with field-induced aggregates, we prove that the additivity rule applies and reads as follows: $\tau_D(H,\varphi_{sep}',\varphi)=\tau_{Dm}(H,\varphi)+\tau_D(0,\varphi_{sep}',\varphi)$ – see Appendix for demonstration. In this case, the dynamic yield stress increment is equal to the magnetic contribution: $\Delta\tau_D(H,\varphi_{sep}',\varphi)=\tau_D(H,\varphi_{sep}',\varphi)-\tau_D(0,\varphi_{sep}',\varphi)=\tau_{Dm}(H,\varphi)\approx\Delta\tau_D(H,0,\varphi)$, and the dynamic yield stress enhancement parameter A_D is zero. However, as already stated, partial expulsion of sepiolite fibers from aggregates composed of iron particles can increase the sepiolite concentration to some value φ_{sep}'' in the suspending fluid surrounding the aggregates and thus increase the dynamic yield stress of the suspending fluid. Such an expulsion is, to some extent, coherent with the three following facts: (a) an increase of the plastic viscosity in the presence of the magnetic field mostly observed for the MRF with φ=20vol% of iron [two right graphs on the bottom raw of Fig. 6]; (b) the initial magnetic susceptibility of the MRF is independent of the amount of sepiolite [Fig. 1], at least suggesting the absence of sepiolite in

the gaps between iron particles inside the aggregates (cf. discussion in Sec. III-A); (c) smaller amount of sepiolite fibers in the location of iron aggregates suggested by SEM-EDX images [Fig. 2e]. In such a case, the enhancement parameter A_D will be proportional to the difference between the off-state dynamic yield stresses taken at concentrations φ_{sep}" and φ_{sep}' (initial concentration in the absence of field):

$$A_D = \frac{\tau_D(0,\varphi_{sep}",\varphi) - \tau_D(0,\varphi_{sep}',\varphi)}{\Delta\tau_D(H,0,\varphi)}. \quad (7)$$

If the concentration difference remains small, $\Delta\varphi_{sep} \equiv \varphi_{sep}" - \varphi_{sep}' << \varphi_{sep}'$, the first order series expansion of the term $\tau_D(0,\varphi_{sep}",\varphi)$ will give the following approximate result:

$$A_D \approx \frac{1}{\Delta\tau_D(H,0,\varphi)} \frac{\partial\tau_D(0,\varphi_{sep}',\varphi)}{\partial\varphi_{sep}'} \Delta\varphi_{sep} \quad (8)$$

The derivative in Eq. (8) is an increasing function of the sepiolite concentration φ_{sep}', as inferred from Fig. 5b. Therefore, equation (8) demonstrates that, in the frames of the present model, the parameter A_D is expected to be a monotonously increasing function of the sepiolite concentration. To have a clearer idea on possible effect of sepiolite concentration on the enhancement parameter A_D, we estimate its value for the extreme case when all sepiolite fibers are squeezed out from the iron particle aggregates such that the sepiolite concentration in the suspending medium is equal to $\varphi_{sep}" = \varphi_{sep}'(1-\varphi)/(1-\varphi/\varphi_a)$, where the internal aggregate volume fraction φ_a is taken to be equal to the maximum volume fraction $\varphi_m \approx 0.5$ of iron particles, as found from off-state viscosity measurements of the MRF without sepiolite addition [Sec. III-D]. Replacing this value of $\varphi_{sep}"$ in Eq. (7) and using a polynomial fit of the experimental data on Fig. 5b for the function $\tau_D(0,\varphi_{sep}',\varphi)$, we get the upper bound estimation of the parameter A_D, which is plotted as function of the sepiolite concentration in Fig. 8d for three considered volume fractions of iron. This simple model predicts a monotonic increase of the upper bound of the enhancement parameter A_D with both the sepiolite concentration φ_{sep}' and the iron concentration φ [Fig. 8d] in contrast to experiments showing a maximum of $A_D(\varphi_{sep}')$ dependency followed by a decrease of A_D with φ_{sep}' and smaller A_D values at the iron concentration φ=20 vol% as compared to φ=10 vol% [Fig. 8b].

Such discrepancy likely comes from the kinetics of the aggregate formation and destruction. In fact, in typical MRFs, the timescale t_a of field-induced aggregation is on the order of a few milliseconds, so is much shorter than the timescale $t_f \sim \dot{\gamma}^{-1}$ of the flow at low

enough shear rates at which the aggregates are still not destroyed by the shear. When $t_a < t_f$, the aggregates are subjected to a rapid growth under magnetic interactions between iron particles followed by their rupture by tensile hydrodynamic forces [51]. Most of the iron particles are expected to form the aggregates. At increasing concentrations φ_{sep}' and φ, the hydrodynamic resistance to motion of iron particles inside the MRF considerably increases. This can make the aggregation timescale $t_a \sim \eta_p(\varphi_{sep}', \varphi)/\tau_m(H, \varphi) \approx \eta_p(\varphi_{sep}', \varphi)/\Delta\tau_D(H, 0, \varphi)$ overcome the flow timescale. In this case the aggregates will not have enough time to grow up to the equilibrium value during the flow timescale t_f and the suspension will likely contain isolated particles not forming the aggregates. The average aggregate size and the average amount of particles constituting the aggregates in the case $t_a > t_f$ are expected to be smaller than those in the case $t_a < t_f$; this should decrease the viscous dissipation generated by aggregates and result in smaller dynamic yield stress at high concentrations φ_{sep}' and φ. The non-monotonous experimental dependence of A_D on φ_{sep}' and φ [Fig. 8b] likely appears as a result of the synergy of two aforementioned mechanisms: (a) enhancement due to expulsion of the sepiolite from aggregates and (b) retarded kinetics of aggregation at increasing viscosity of the suspending medium.

From the practical point of view, the formulation containing φ=10 vol% of iron and φ_{sep}=4 vol% of sepiolite seems to combine a perfect sedimentation stability [upper curve in Fig. 3b] with reasonable values of the plastic viscosity (only by a factor of two larger than the viscosity of the MRF with φ=10 vol% and φ_{sep}=0 vol%, cf. Fig. 5a), weak off-state static yield stress (only ~5 Pa) and a non-negligible static and dynamic yield stress enhancement ($A_S \approx 30\%$ and $A_D \approx 60\%$).

IV. Conclusions

This work is focused on the characterization and magnetorheological study of the MRF composed of iron particles and sepiolite fibers, used as a thickening agent allowing improvement of sedimentation stability of the MRF. The work is aimed at (a) understanding the effect of the sepiolite addition on the MR response; and (b) finding an appropriate formulation allowing a good sedimentation stability keeping a relatively low off-state viscosity and providing an enhanced MR effect. The coupling of different characterizations

(magnetization measurements, SEM-EDX, rheometry) and theoretical estimations (some of which are based on the homogenization approach of Château *et al*. [44]) have allowed us to draw the following conclusions:

1. The magnetorheology of the MRFs with sepiolite addition is qualitatively similar to that of the MRFs without sepiolite: at shear rates $\dot{\gamma}$ >25 s^{-1} the flow curves are satisfactorily fitted by the Bingham rheological law with the dynamic yield stress and the plastic viscosity depending on the sepiolite concentration φ_{sep}, while in low shear domain the suspension develops a static yield stress also depending on φ_{sep}. The static or dynamic yield stress enhancement with sepiolite addition is analyzed through enhancement parameters A_S or A_D. In our experimental conditions, the effect of φ_{sep} is unlikely due to the change of the structure strength or change in solid friction between iron particles, as suggested by Lopez-Lopez *et al*. [13] and Bombard *et al*. [14] because the sepiolite fibers seem not to be present in the gaps between iron particles in the aggregates.
2. The static yield stress enhancement parameter A_S is found to progressively grow with both sepiolite and iron concentrations. This is explained in frames of a qualitative theoretical model assuming a friction (between gap-spanning aggregates composed of iron particles and the sepiolite-oil viscoplastic matrix) appearing as a result of non-affine deformation of aggregates during shear. This friction is enhanced with increasing sepiolite and iron concentrations but exhibits a non-monotonic dependency on the applied magnetic field qualitatively supported by the same model.
3. The dynamic yield stress enhancement parameter A_D shows an initial increase with the sepiolite concentration followed by a decrease. This parameter appears to be smaller for the iron concentration φ=20 vol% than for φ=10 vol%. The initial increase of A_D with φ_{sep} is explained by a partial expulsion of the sepiolite fibers from the iron aggregates – the hypothesis supported to some extent by magnetization measurements, SEM-EDX and by off-state rheometry. The decrease of A_D with φ_{sep} and with φ remains unclear and is tentatively explained by a retarded kinetics of aggregation at increasing viscosity of the suspending medium, which likely reduces the average aggregate size and population of iron particles constituting the aggregates.
4. We find that the formulation containing φ=10 vol% of iron and φ_{sep}=4 vol% of sepiolite seems to combine a perfect sedimentation stability with moderate values of the plastic viscosity (only by a factor of two larger than the viscosity of the MRF without

sepiolite), weak off-state static yield stress (only ~5 Pa) and a non-negligible static and dynamic yield stress enhancement (A_S≈30% and A_D≈60% at H=30.6 kA/m).

The results of the present paper are expected to be interesting for applications of iron-sepiolite MRFs in MR devices requiring good sedimentation stability without loss of the MR effect.

Supplementary Material

See supplementary material for magnetization data in emu/g units; flow curves in double logarithmic scale; static and dynamic yield stress, as well as yield stress increments as function of the applied magnetic field and of the sepiolite volume fraction.

Acknowledgments

This work has been supported by the French government, piloted by the National Research Agency (ANR) in frames of the project Future Investments UCAJEDI, ref n° ANR-15-IDEX-01 (projects RheoCimPl and RheoGels). JAM acknowledges Brazilian CNPq for the postdoctoral fellowship (grant n° 203100/2014). TP acknowledges funding from Czech Ministry of Education, Youth and Sports of the Czech Republic – Program NPU I (LO1504). The authors thank Dr. Georges Bossis for helpful discussions, Dr. Sophie Pagnotta and Dr. François Orange (Common Center of Applied Microscopy, University of Nice-Sophia Antipolis) for their help with the electron microscopy.

Appendix. Proof of the yield stress additivity rule using the homogenization approach

The homogenization approach is typically applied to suspensions of hard spheres dispersed in a non-Newtonian suspending fluid at a volume fraction φ. This approach postulates that the viscosity of such suspensions can be estimated as a product of the relative viscosity $g(\varphi) \equiv \eta(\varphi)/\eta(0)$ of a suspension in a Newtonian solvent and the viscosity of a non-Newtonian suspending fluid taken at an average local shear rate [44, 45]. In this Appendix, the homogenization approach is extended to the case of suspensions of magnetic hard spheres dispersed in a non-Newtonian suspending fluid (sepiolite-oil mixture in our case).

Firstly, in the case of a Newtonian suspending fluid with a constant viscosity $\eta(0)$, the shear stress versus shear rate dependency at high enough shear rates and in the presence of a magnetic field often satisfies the Bingham rheological equation (2), which can be written in the following form:

$$\tau = \eta(0) g(\varphi)\dot{\gamma} + \tau_{Dm}(\varphi) = \eta(0)\dot{\gamma}\left(g(\varphi) + \frac{\tau_{Dm}(\varphi)}{\tau(0)} \right), \qquad \text{(A-1)}$$

where $\tau(0) = \eta(0)\dot{\gamma}$ is the shear stress in Newtonian suspending fluid sheared at a global shear rate $\dot{\gamma}$ and $\tau_{Dm}(\varphi)$ is the stress contribution coming from enhanced hydrodynamic dissipation on field-induced particle aggregates. The aggregate size decreases with an increasing shear rate making shear rate disappear from the expression for $\tau_{Dm}(\varphi)$ and thus allowing to associate $\tau_{Dm}(\varphi)$ with a dynamic yield stress of the MRF [7, 51].

Secondly, according to the homogenization approach, the average local shear rate $\dot{\gamma}_{loc}$ in the suspending fluid between hard spheres is estimated assuming that the energy dissipation only takes place in the suspending fluid, while solid friction between particles is absent. This assumption imposes an equality of the energy *w* dissipated (per unit time and unit suspension volume) in the whole suspension and the energy w_{loc} dissipated in the suspending fluid. These both energies for Newtonian suspending fluid read:

$$w = \tau\dot{\gamma} = \eta(0)\dot{\gamma}^2\left(g(\varphi) + \frac{\tau_{Dm}(\varphi)}{\tau(0)} \right), \qquad \text{(A-2a)}$$

$$w_{loc} = (1-\varphi)\eta(0)\dot{\gamma}_{loc}{}^2 . \qquad \text{(A-2b)}$$

Equalizing right-hand sides of Eqs. (A-2a) and (A-2b), we get the following expression for the local shear rate:

$$\dot{\gamma}_{loc} = \dot{\gamma}\left(\frac{g(\varphi) + \tau_{Dm}(\varphi)/\tau(0)}{1-\varphi} \right)^{1/2} . \qquad \text{(A-3)}$$

Thirdly, we have now to consider the real suspending fluid of our MRF, which at high enough shear rates exhibits a Bingham behavior [Eq. (2), Fig. 4] with a dynamic yield stress denoted by $\tau_{D0} = \tau_D(\varphi_{sep}', 0)$. The viscosity of the Bingham suspending fluid at the local shear rate reads:

$$\eta(\dot{\gamma}_{loc}) = \eta_0 + \frac{\tau_{D0}}{\dot{\gamma}_{loc}}, \qquad \text{(A-4)}$$

recalling that η_0 in our case is the viscosity of a Newtonian solvent (silicone oil) of the sepiolite-oil mixture.

Finally, replacing in Eq. (A-1) the viscosity $\eta(0)$ of a Newtonian suspending fluid by a viscosity $\eta(\dot{\gamma}_{loc})$ of a non-Newtonian suspending fluid at local shear rate, making use of Eqs. (A-3), (A-4), we get the following expression for the shear stress versus shear rate dependency for the MRF with magnetic particles dispersed in a Bingham suspending fluid:

$$\tau = \tau_{D0}\left[(1-\varphi)\left(g(\varphi)+\frac{\tau_{Dm}(\varphi)}{\tau^*}\right)\right]^{1/2} + \eta_0\dot{\gamma}\left(g(\varphi)+\frac{\tau_{Dm}(\varphi)}{\tau^*}\right), \qquad \text{(A-5a)}$$

$$\tau^* = \tau_{D0}\left[\frac{1-\varphi}{g(\varphi)+\tau_{Dm}(\varphi)/\tau^*}\right]^{1/2} + \eta_0\dot{\gamma}, \qquad \text{(A-5b)}$$

with τ^* being found by solving a transcendent equation (A-5b).

We check that equation (A-5a) reduces to well-known results as follows in the two limiting cases: (a) the Newtonian suspending fluid with $\tau_{D0}=0$ [3] and; (b) zero magnetic field implying $\tau_{Dm}(\varphi)$=0 [45]:

$$\tau = \eta_0 g(\varphi)\dot{\gamma} + \tau_{Dm}(\varphi) \text{ at } \tau_{D0}=0, \qquad \text{(A-6a)}$$

$$\tau = \tau_{D0}\left[(1-\varphi)g(\varphi)\right]^{1/2} + \eta_0 g(\varphi)\dot{\gamma} \text{ at } \tau_{Dm}=0. \qquad \text{(A-6b)}$$

Notice that in our experiments, the flow curves of both oil-sepiolite mixtures and of the MRF are well interpolated by the Bingham law only at relatively high shear rates (at least at $\dot{\gamma} > 25\ \text{s}^{-1}$, see Figs. 4, 6). At such condition, the above analysis can be considered as valid when the following strong inequalities hold: $\tau_{D0} << \eta_0\dot{\gamma}$ and $\tau_{Dm}(\varphi) << \eta_0\dot{\gamma}$. Thus, keeping the leading terms on τ_{D0} and $\tau_{Dm}(\varphi)$ in Eqs. (A-5a), (A-5b), we get the final approximate expression for the stress versus shear rate dependency of the MRF with a Bingham suspending fluid:

$$\tau \approx \tau_{D0}\left[(1-\varphi)g(\varphi)\right]^{1/2} + \eta_0 g(\varphi)\dot{\gamma} + \tau_{Dm}(\varphi). \qquad \text{(A-7)}$$

The two first terms in the right-hand side of the last equation stand for the contribution of the Bingham suspending fluid, while the third term is the dynamic yield stress coming from field-induced aggregation and thus depending on the magnetic field. The equation (A-7) proves therefore an additivity rule for the dynamic yield stress, at least in the high shear limit for which the Bingham law holds.

References

[1] Park, B. J., F.F Fang, and H. J Choi, "Magnetorheology: materials and application". Soft Matter **6**(21), 5246-5253 (2010).

[2] de Vicente, J., D. J. Klingenberg, and R. Hidalgo-Alvarez, "Magnetorheological fluids: A review," Soft Matter **7**, 3701–3710 (2011).

[3] Bossis, G., O Volkova, S Lacis, and A Meunier, "Magnetorheology: fluids, structures and rheology," Lecture Notes in Physics, **594**, 202-232 (2002).

[4] Jolly, M. R., J. W Bender, and J. D. Carlson, "Properties and applications of commercial magnetorheological fluids," J. Intell. Material Syst. Struct. **10**(1), 5-13 (1999).

[5] Wang, J., and G. Meng, "Magnetorheological fluid devices: principles, characteristics and applications in mechanical engineering," Proc. Inst. Mech. Eng. L: Journal of Materials: Design and Applications, **215**(3), 165-174 (2001).

[6] Carlson, J. D., D. M. Catanzarite, and K. A. St. Clair, "Commercial magneto-rheological fluid devices," Int. J. Mod. Phys. B **10**, 2857–2865 (1996).

[7] Shulman, Z. P., and W. I. Kordonsky, Magnetorheological Effect (Nauka i Tehnika, Minsk, 1982) [in Russian].

[8] López-López, M. T., J. D. G Durán, A. V. Delgado, and F. González-Caballero, "Stability and magnetic characterization of oleate-covered magnetite ferrofluids in different nonpolar carriers". J. Colloid Interface Sci. **291**(1), 144-151 (2005).

[9] Hato, M. J., H.J Choi, H.H. Sim, B.O. Park, and S.S. Ray, "Magnetic carbonyl iron suspension with organoclay additive and its magnetorheological properties". Colloids Surf. A **377**(1), 103-109 (2011).

[10] Hong, C. H., Y.D. Liu, and H.J. Choi, "Carbonyl iron suspension with halloysite additive and its magnetorheology," Appl. Clay Sci. **80**, 366-371 (2013).

[11] Chae, H. S., S.H. Piao, A. Maity, and H. J. Choi, "Additive role of attapulgite nanoclay on carbonyl iron-based magnetorheological suspension," Colloid and Polym. Sci. **293**(1), 89-95 (2015).

[12] Piao, S. H., W. L. Zhang, and H.J. Choi, "Magnetic carbonyl iron suspension with sepiolite additive and its magnetorheological property". IEEE Trans. Magn. **50**(1), 1-4 (2014).

[13] López-López, M. T., A, Gómez-Ramírez, J.D. Durán, and F, González-Caballero, "Preparation and characterization of iron-based magnetorheological fluids stabilized by addition of organoclay particles". Langmuir **24**(14), 7076-7084 (2008).

[14] Bombard, A. J., F. R. Gonçalves, J. R. Morillas, and J. de Vicente, "Magnetorheology of dimorphic magnetorheological fluids based on nanofibers". Smart Mater. Struct. **23**(12), 125013 (2014).

[15] Kim, M. W., W. J. Han, Y. H. Kim, and H. J. Choi. "Effect of a hard magnetic particle additive on rheological characteristics of microspherical carbonyl iron-based magnetorheological fluid". Colloids Surf. A **506**, 812-820 (2016).

[16] Kim, M. H., K. Choi, J. Do Nam, and H. J. Choi, "Enhanced magnetorheological response of magnetic chromium dioxide nanoparticle added carbonyl iron suspension". Smart Mater. Struct. **26**(9), 095006 (2017).

[17] Ngatu, G. T., N. M. Wereley, J.O. Karli, and R.C. Bell, "Dimorphic magnetorheological fluids: exploiting partial substitution of microspheres by nanowires". Smart Mater. Struct. **17**(4), 045022 (2008).

[18] Sedlacik, M., Pavlínek, V., Vyroubal, R., Peer, P., & Filip, P. (2013). A dimorphic magnetorheological fluid with improved oxidation and chemical stability under oscillatory shear. Smart Mater. Struct. **22**(3), 035011.

[19] Jiang, W., Y, Zhang, S, Xuan, C. Guo, and X, Gong, "Dimorphic magnetorheological fluid with improved rheological properties" J. Magn. Magn. Mater. **323**(24), 3246-3250 (2011).

[20] de Vicente, J., J. P. Segovia-Gutiérrez, E. Andablo-Reyes, F. Vereda, and R. Hidalgo-Álvarez, "Dynamic rheology of sphere-and rod-based magnetorheological fluids," J. Chem. Phys. 131(19), 194902 (2009).

[21] Kuzhir, P., M.T. López-López, and G. Bossis, "Magnetorheology of fiber suspensions. II. Theory," J Rheol. **53**(1), 127-151 (2009).

[22] Fang, F. F., Y. D. Liu, H. J. Choi, and Y. Seo, "Core–shell structured carbonyl iron microspheres prepared via dual-step functionality coatings and their magnetorheological response". ACS Appl. Mater. Interfaces **3**(9), 3487-3495 (2011).

[23] Rautureau, M., and C, Tchoubar, "Structural analysis of sepiolite by selected area electron difraction--relations with physico-chemical properties," Clays and Clay Miner. **24**, 43–49 (1976).

[24] Serna, C., J. L. Ahlrichs, and J. M. Serratosa, "Folding in sepiolite crystals," Clays Clay Miner. **23**(6), 452-457 (1975).

[25] Marins, J. A., F. Giulieri, B. G. Soares, and G, Bossis, "Hybrid polyaniline-coated sepiolite nanofibers for electrorheological fluid applications," Synth. Met. **185**, 9-16 2013.

[26] Marins, J. A., A. Mija, J. M. Pin, F. Giulieri, B. G. Soares, N. Sbirrazzuoli, and G. Bossis, "Anisotropic reinforcement of epoxy-based nanocomposites with aligned magnetite–sepiolite hybrid nanofiller," Compos. Sci. Technol. **112**, 34-41 (2015).

[27] López-López, M. T., P. Kuzhir, G. Bossis, and P. Mingalyov, "Preparation of well-dispersed magnetorheological fluids and effect of dispersion on their magnetorheological properties," Rheol. Acta **47**(7), 787-796 (2008).

[28] López-López, M. T., P. Kuzhir, and G. Bossis, "Magnetorheology of fiber suspensions. I. Experimental," J. Rheol. **53**(1), 115-126 (2009).

[29] Jiles, D., Introduction to Magnetism and Magnetic Materials (Chapman and Hall, London, 1991).

[30] See supplementary material for deposit file "Supplemental-Material.pdf": Magnetization data in emu/g units; Flow curves in double logarithmic scale; Static and dynamic yield stress, as well as yield stress increments as function of the applied magnetic field and of the sepiolite volume fraction.

[31] Danan, H., A. Herr, and A. J. P. Meyer, "New determinations of the saturation magnetization of nickel and iron," J. Appl. Phys. **39**(2), 669-670 (1968).

[32] de Vicente, J., G. Bossis, S. Lacis, and M. Guyot, "Permeability measurements in cobalt ferrite and carbonyl iron powders and suspensions," J. Magn. Magn. Mater. **251**(1), 100-108 (2002).

[33] López-López, M. T., P. Kuzhir, J. Caballero-Hernandez, L. Rodríguez-Arco, J.D. Durán, and G. Bossis, "Yield stress in magnetorheological suspensions near the limit of maximum-packing fraction," J. Rheol. **56**(5), 1209-1224 (2012).

[34] Borbath, T., S. Günther, D. Yu Borin, Th. Gundermann, and S. Odenbach, "XmCT analysis of magnetic fieldinduced phase transitions in magnetorheological elastomers," Smart Mater. Struct. **21**, 105018 (2012).

[35] Tao, R., and J. M. Sun, "Three-dimensional structure of induced electrorheological solid," Phys. Rev. Lett. **67**, 398–401 (1991).

[36] Hubbe, M. A., "Flocculation and redispersion of cellulosic fiber suspensions: A review of effect of hydrodynamic shear and polyelectrolytes," BioResources **2**, 296–331 (2007).

[37] Björkman, U., "Break-up of suspended fibre networks," Nord. Pulp Pap. Res. J. **18**, 32–37 (2003).

[38] Karppinen, A., T. Saarinen, J. Salmela, A. Laukkanen, M. Nuopponen, and J. Seppälä, "Flocculation of microfibrillated cellulose in shear flow," Cellulose **19**, 1807–1819 (2012).

[39] Larson, R. G., The Structure and Rheology of Complex Fluids (Oxford University Press, New York, 1999).

[40] Rahatekar, S. S., K. K. Koziol, S. R. Kline, E. K. Hobbie, J. W. Gilman, and A. H. Windle, "Length-dependent mechanics of carbon nanotube networks," Adv. Mater. **21**, 874–878 (2009).

[41] Cui, H., and J. R. Grace, "Flow of pulp fibre suspension and slurries: A review," Int. J. Multiphase Flow **33**, 921–934 (2007).

[42] Servais, C., J. A. E. Månson, and S. Toll, "Fiber–fiber interaction in concentrated suspensions: Disperse fibers," J. Rheol. **43**, 991–1004 (1999).

[43] Switzer III, L. H., and D. J. Klingenberg, "Rheology of sheared flexible fiber suspensions via fiber-level simulations," J. Rheol. **47**, 759–778 (2003).

[44] Chateau, X., G. Ovarlez, and K.L. Trung, "Homogenization approach to the behavior of suspensions of noncolloidal particles in yield stress fluids". J. Rheol. **52**(2), 489-506 (2008).

[45] Ovarlez, G., F. Mahaut, S. Deboeuf, N. Lenoir, S. Hormozi, and X. Chateau, " Flows of suspensions of particles in yield stress fluids," J. Rheol. **59**(6), 1449-1486 (2015).

[46] Maron, S. H., and P.F. Pierce, "Application of Ree-Eyring generalized flow theory to suspensions of spherical particles," J. Colloid Sci. **11**(1), 80-95, (1956).

[47] Barnes, H. A. "The yield stress—a review or 'παντα ρει'—everything flows?," J. Non-Newtonian Fluid Mech. **81**(1-2), 133-178 (1999).

[48] Gomez-Ramırez, A., P. Kuzhir, M. T. Lopez-Lopez, G. Bossis, A. Meunier, and J. D. G. Duran, "Steady shear flow of magnetic fiber suspensions: Theory and comparison with experiments," J. Rheol. **55**, 43–67 (2011).

[49] Bossis, G., E. Lemaire, O. Volkova, and H. Clercx, "Yield stress in magnetorheological and electrorheological fluids: A comparison between microscopic and macroscopic structural models," J. Rheol. **41**, 687–704 (1997).

[50] D.J. Klingenberg, "Simulation of the dynamic oscillatory response of electrorheological suspensions: demonstration of a relaxation mechanism", J. Rheol. **37** (1993) 199–214.

[51] Martin, J. E., and R. Anderson, "Chain model of electrorheology," J. Chem. Phys. **104**, 4814–4826 (1996).